

Motion Artifact Reduction in Photoplethysmography using Bayesian Classification for Physical Exercise Identification

Giorgio Biagetti, Paolo Crippa, Laura Falaschetti, Simone Orcioni and Claudio Turchetti

*DII – Dipartimento di Ingegneria dell'Informazione, Università Politecnica delle Marche,
Via Brecce Bianche 12, I-60131 Ancona, Italy*

Keywords: Photoplethysmography, PPG, Motion Artifact Reduction, Heart Rate, Bayesian Classification, Identification, GMM, Expectation Maximization, Karhunen-Loève Transform.

Abstract: Accurate heart rate (HR) estimation from photoplethysmography (PPG) recorded from subjects' wrist when the subjects are performing various physical exercises is a challenging problem. This paper presents a framework that combines a robust algorithm capable of estimating HR from PPG signal with subjects performing a single exercise and a physical exercise identification algorithm capable of recognizing the exercise the subject is performing. Experimental results on subjects performing two different exercises show that an improvement of about 50% in the accuracy of HR estimation is achieved with the proposed approach.

1 INTRODUCTION

Photoplethysmography (PPG) is a non invasive technique to estimate the heart rate (HR) by measuring the blood flow at the surface of the skin. In wearable devices for fitness and/or daily activities this signal needs to be monitored when motion is always present.

The subjects' hand movements during intensive physical exercise cause a strong motion artifact (MA) that corrupts PPG signal, making HR monitoring from wrist devices a challenging problem.

Many signal processing techniques have been proposed to remove MA from raw PPG signal. The most common are: independent component analysis (Kim and Yoo, 2006), adaptive filtering techniques (Foo, 2006; Gibbs et al., 2005), Kalman filtering (Lee et al., 2010), wavelet based methods (Raghuram et al., 2010), empirical mode decomposition (Raghuram et al., 2014; Raghuram et al., 2012). More recently combinations of a number of techniques have been successfully used (Ram et al., 2012; Zhang et al., 2015).

However, although an HR estimation with an average absolute error less than 2 beats per minute (BPM) can be obtained by these latest techniques, such a performance is limited to PPG signals recorded from subjects during fast running.

Thus accurate HR estimation from PPG recorded from subjects' wrist when the subjects are performing various physical exercises, such as fast running,

weightlifting, or jumping, remains a challenge.

This paper focuses on this aspect, namely MA reduction in PPG when subjects perform various physical exercises. In particular a physical exercise identification algorithm, based on Bayesian classification and truncated Karhunen-Loève transform (KLT) representation, which is able to recognize the physical exercise the subject is performing, is adopted to this end. This algorithm is combined with a robust artifact reduction algorithm, CARMA (Bacà et al., 2015), which can be optimized for a single physical exercise by setting a specific tracking model. Once a set of different tracking models are derived, the exercise the subject is performing is automatically selected by the identification algorithm.

The rest of the paper is organized as follows. Section 2 reviews the CARMA algorithm. Section 3 reports the physical exercise identification algorithm. Section 4 describes the framework adopted for MA reduction combining both CARMA and the physical exercise identification algorithm. Section 5 discusses experimental results. Conclusion is given in the last section.

2 CARMA ALGORITHM

The CARMA algorithm has proven to be very effective for HR monitoring from PPG signals with subjects performing a single physical exercise.

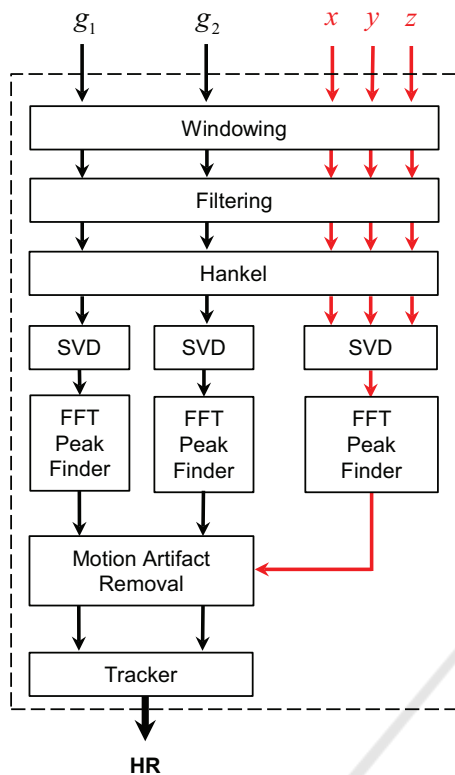


Figure 1: Flow chart of CARMA algorithm (g_1 and g_2 are the PPG channels, x, y, z are the 3-axis accelerometer signals).

A flow chart of the algorithm is shown in Fig. 1. It consists of the following steps: *i*) pre-processing of PPG and accelerometer signals, *ii*) singular value decomposition (SVD), *iii*) peak detection of the FFTs, *iv*) MA reduction, *v*) tracking of the HR.

2.1 Review of Subspace Decomposition Approach and Tracking

Given the accelerometer signals x, y, z the main objective of the algorithm is to determine the corresponding subspace $\langle S \rangle$ they belong to, that is a basis S that generates $\langle S \rangle$. To this end let $X = [x^{(1)} \dots x^{(L)}]$, $Y = [y^{(1)} \dots y^{(L)}]$, $Z = [z^{(1)} \dots z^{(L)}]$ be the Hankel data matrices of the three signals respectively, then the complete matrix of sample signals

$$H = [XYZ] \quad (1)$$

can be approximated by the SVD as

$$H \cong \sum_{i=1}^P \lambda_i s_i r_i^T, \quad (2)$$

where λ_i are the singular values in decreasing order and s_i, r_i the corresponding left and right singular vectors.

This approximation is equivalent to assume the signals are in the subspace

$$\langle S \rangle = \text{span}(s_1 \dots s_P), \quad (3)$$

generated by the basis $S = [s_1 \dots s_P]$ where $s_1 \dots s_P$ are the most significant components of the motion signal, and $\langle S \rangle$ represents the subspace of motion signals (SMS).

Considering the following model for the PPG signal

$$g = m + e, \quad (4)$$

where e is the HR signal, m the artifact and g the PPG signal, as m belongs to the subspace $\langle S \rangle$, then the corresponding Hankel data matrix G can be written as

$$G = SA + E. \quad (5)$$

Assuming the component SB of E belonging to the subspace $\langle S \rangle$ is negligible when comparing with the artifact component SA , that is

$$E \simeq S_{\perp} B_{\perp}, \quad (6)$$

where $S_{\perp} = [s_{P+1} \dots s_N]$ is orthogonal to S , it results

$$G = SA + E \simeq SA + S_{\perp} B_{\perp}. \quad (7)$$

Now let

$$G = U \Sigma V^T \quad (8)$$

be the SVD of G , where $U = [u_1 \dots u_N]$, $V = [v_1 \dots v_L]$, and Σ is the matrix of singular values, then the two components SA, E can be derived by selecting the vectors u_i that are the closest to the subspace $\langle S \rangle$.

In order to define a physically meaningful distance between these vectors, both s_i and u_i are characterized by the central frequency of their main spectral peak, and the distance between a vector u_i and the subspace $\langle S \rangle$ is defined as the shortest distance between the vector u_i and any of the s_i .

The set $(u_{i_1} \dots u_{i_Q})$ is then chosen such that the corresponding distances are below a given threshold ϑ , so that the subspace $\langle U_q \rangle = \text{span}(u_{i_1} \dots u_{i_Q})$ is the closest to the artifact subspace $\langle S \rangle$.

As a consequence the following decomposition

$$G = [U_q U_d] \begin{bmatrix} \Sigma_q & 0 \\ 0 & \Sigma_d \end{bmatrix} \begin{bmatrix} V_q^T \\ V_d^T \end{bmatrix} \\ = U_q \Sigma_q V_q^T + U_d \Sigma_d V_d^T, \quad (9)$$

with $U_q = [u_{i_1} \dots u_{i_Q}]$, $U_d = [u_{i_{Q+1}} \dots u_{i_N}]$, holds.

Assuming the vectors $(u_{i_1} \dots u_{i_Q})$ belong to the subspace $\langle S \rangle$ and posing

$$\Sigma_q V_q^T = [b^{(1)} \dots b^{(L)}] \quad (10)$$

it follows that every column of the matrix

$$U_q \Sigma_q V_q^T = [U_q b^{(1)} \dots U_q b^{(L)}] \quad (11)$$

belong to $\langle S \rangle$. Finally, comparing (7) with (9) yields

$$\begin{cases} SA \simeq U_q \Sigma_q V_q^T \\ E \simeq U_d \Sigma_d V_d^T \end{cases}. \quad (12)$$

Having derived the representation of E , then the HR can be found as the dominant frequency of the first column of U_d alone.

Whilst the artifact removal so performed is usually very good, a frequency tracking algorithm is necessary to further reduce HR estimation error and to combine the signals from the two available PPG channels.

First a check is made to determine if the extracted frequency is a harmonic of the HR, and it is halved or doubled according to the result being more likely. This is done exploiting a rough estimate of the joint probability density function (pdf) of the HR versus the motion artifact frequency (MAF).

Then, to select the best of the two PPG channels, the one that is closest to the previous estimate is chosen. Let e_{t-1} be the previous HR estimate, the current estimate e_t is found by

$$e_t = \kappa e_{t-1} + (1 - \kappa) f_t, \quad (13)$$

where f_t is the frequency of the selected peak, $\kappa \in [0, 1]$ is a weighting factor that increases as the distance of f_t from e_{t-1} increases and can be adjusted to filter out spurious estimates while simultaneously tracking relatively rapid HR variations.

The algorithm previously reviewed behaves well for a single physical exercise, however it fails when subjects perform various physical exercises, as it will be shown in Sect. 5. To remove this limitation a set Γ of different tracking models, specifically optimized for various physical exercises, can be derived and automatically selected by a physical exercise identification algorithm.

3 PHYSICAL EXERCISE IDENTIFICATION

The algorithm developed in this section follows the approach reported in (Biagetti et al., 2015) as it was successfully adopted in the field of speaker identification.

3.1 Bayesian Classification

Let us refer to a frame $\xi[n]$, $n = 0, \dots, N - 1$, containing features extracted from the accelerometer signals.

We assume that the observations for all physical exercises that need to be identified, are acquired and divided in two sets, \mathcal{W} for training and \mathcal{Z} for testing.

For Bayesian classification, a group of Γ exercises is represented by the probability density functions (pdfs)

$$p_\gamma(\xi) = p(\xi | \theta_\gamma) \quad , \quad \gamma = 1, 2, \dots, \Gamma, \quad (14)$$

where θ_γ are the parameters to be estimated during training, $\xi \in \mathcal{W}$. Thus we can define the vector

$$p = [p_1(\xi), \dots, p_\Gamma(\xi)]^T. \quad (15)$$

The objective of classification is to find the model θ_γ corresponding to the exercise γ which has the maximum a posteriori probability for a given frame $\xi \in \mathcal{Z}$. Formally:

$$\begin{aligned} \hat{\gamma}(\xi) &= \operatorname{argmax}_{1 \leq \gamma \leq \Gamma} \{p(\theta_\gamma | \xi)\} \\ &= \operatorname{argmax}_{1 \leq \gamma \leq \Gamma} \left\{ \frac{p(\xi | \theta_\gamma) p(\theta_\gamma)}{p(\xi)} \right\}. \end{aligned} \quad (16)$$

Assuming equally likely exercises (i.e. $p(\theta_\gamma) = 1/\Gamma$) and noting that $p(\xi)$ is the same for all exercise models, the Bayesian classification is equivalent to

$$\hat{\gamma}(\xi) = \operatorname{argmax}_{1 \leq \gamma \leq \Gamma} \{p_\gamma(\xi)\}. \quad (17)$$

Thus Bayesian identification reduces to solving the problem stated by (17).

The most generic statistical model one can adopt for $p(\xi | \theta_\gamma)$ is the Gaussian mixture model (GMM) (Reynolds and Rose, 1995). The GMM for the single exercise is a weighted sum of F components densities and given by the equation

$$p(\xi | \theta) = \sum_{i=1}^F \alpha_i \mathcal{N}(\xi | \mu_i, C_i) \quad (18)$$

where α_i , $i = 1, \dots, F$ are the mixing weights, and $\mathcal{N}(\xi | \mu_i, C_i)$ represents the density of a Gaussian distribution with mean μ_i and covariance matrix C_i . It is worth noting that α_i must satisfy $0 \leq \alpha_i \leq 1$ and $\sum_{i=1}^F \alpha_i = 1$.

θ (the index γ is omitted for the sake of notation simplicity) is the set of parameters needed to specify the Gaussian mixture, defined as

$$\theta = \{\alpha_1, \mu_1, C_1, \dots, \alpha_F, \mu_F, C_F\}. \quad (19)$$

The usual choice for solving estimate of the mixture parameters is the expectation maximization (EM) algorithm.

The EM algorithm is based on the interpretation of \mathcal{W} as incomplete data and \mathcal{H} as the missing part of the complete data $\mathcal{X} = \{\mathcal{W}, \mathcal{H}\}$. In general the EM algorithm computes a sequence of parameter estimates $\{\hat{\theta}(p), p = 0, 1, \dots\}$ by iteratively performing two steps:

- *Expectation step*: compute the expected value of the complete log-likelihood, given the training set \mathcal{W} and the current parameter estimate $\hat{\theta}(p)$. The result is the so-called *auxiliary function*

$$Q(\theta|\hat{\theta}(p)) = E \{ \log [p(\mathcal{W}, \mathcal{H}|\theta)] | \mathcal{W}, \hat{\theta}(p) \} . \quad (20)$$

- *Maximization step*: update the parameter estimate

$$\hat{\theta}(p+1) = \underset{\theta}{\operatorname{argmax}} \{ Q(\theta|\hat{\theta}(p)) \} \quad (21)$$

by maximizing the Q -function.

Recently, Figueiredo *et al.* (Figueiredo and Jain, 2002) suggested an unsupervised algorithm for learning a finite mixture model from multivariate data, that overcomes the main lacks of the standard EM approach, i.e. sensitiveness to initialization and selection of number F of components.

This algorithm integrates both model estimation and component selection, i.e. the ability of choosing the best number of mixture components F according to a predefined minimization criterion, in a single framework.

3.2 Bayesian Classification by Truncated KLT Representation

For a sampling rate of 125 Hz a good choice of N is 400 (Zhang *et al.*, 2015). Although the Figueiredo's EM algorithm behaves well with multivariate random vectors, a too large amount of training data would be necessary to estimate the pdf $p(\xi | \theta_\gamma)$ and, in any case, with such a dimension the estimation problem is impractical.

In order to face the problem of dimensionality, the usual choice (Jain *et al.*, 2000) is to reduce the vector ξ to a vector k_M of lower dimension by a linear non-invertible transform H (a rectangular matrix) such that

$$k_M = H \xi , \quad (22)$$

where $\xi \in \mathbb{R}^N$, $k_M \in \mathbb{R}^M$, $H \in \mathbb{R}^{M \times N}$, and $M \ll N$.

It is well known that, among the allowable linear transforms $H : \mathbb{R}^N \rightarrow \mathbb{R}^M$, the Karhunen-Loève transform truncated to $M < N$ orthonormal basis functions, is the one that ensures the minimum mean square error.

To this end, let us consider the vector $\xi[n]$, $n = 0, \dots, N-1$, as an observation of the $N \times 1$ real random vector $\xi = [\xi_1, \dots, \xi_N]^T$ with autocorrelation function $R_{\xi\xi}$.

Once $R_{\xi\xi}$ is estimated, an orthonormal set $\{\phi_1, \dots, \phi_N\}$, can be derived so that the KLT of ξ is given by the couple of equations (Fukunaga, 1990)

$$k = \Phi^T \xi , \quad (23)$$

$$\xi = \Phi k , \quad (24)$$

where $k = [k_1, \dots, k_N]^T$ is the transformed random vector.

In order to reduce the dimension of such a representation, let us rewrite (24) as:

$$\xi = \Phi k = \Phi_M k_M + \Phi_\eta k_\eta = \xi_M + \eta_\xi , \quad (25)$$

where $\Phi = [\Phi_M, \Phi_\eta]$, being $\Phi_M = [\phi_1, \dots, \phi_M]$ the eigenvectors corresponding to the most significant eigenvalues, $k_M \in \mathbb{R}^M$.

In (25)

$$\xi_M = \Phi_M k_M \quad (26)$$

is the truncated expansion, and

$$\eta_\xi = \Phi_\eta k_\eta \quad (27)$$

is the error or residual.

The truncation is equivalent to the approximations

$$\xi \approx \xi_M , \quad k \approx k_T = \begin{pmatrix} k_M \\ 0 \end{pmatrix} , \quad (28)$$

thus, as k_M is given by

$$k_M = \Phi_M^T \xi , \quad (29)$$

comparing with (22) yields $H = \Phi_M^T$.

Given a group of Γ exercises, let us define the pdfs

$$p_\gamma(k_T) = p(k_T | \theta_\gamma) , \quad \gamma = 1, 2, \dots, \Gamma , \quad (30)$$

where k_T is the truncation of k . Consequently the vector

$$\tilde{p} = [p_1(k_T), \dots, p_\Gamma(k_T)]^T \quad (31)$$

represents an approximation of the vector p in (15). Thus (17) becomes:

$$\hat{\gamma}(\xi) = \underset{1 \leq \gamma \leq \Gamma}{\operatorname{argmax}} \{ p_\gamma(k_T) \} . \quad (32)$$

However, due to truncation, we have

$$p_\gamma(k_T) = p_\gamma(k_M) \delta(k_\eta) , \quad (33)$$

so it results

$$\begin{aligned} \hat{\gamma}(\xi) &= \underset{1 \leq \gamma \leq \Gamma}{\operatorname{argmax}} \{ p_\gamma(k_M) \delta(k_\eta) \} \\ &= \underset{1 \leq \gamma \leq \Gamma}{\operatorname{argmax}} \{ p_\gamma(k_M) \} . \end{aligned} \quad (34)$$

As you can see comparing (34) with (17), the dimensionality of classification problem is reduced from N to M , with $M < N$.

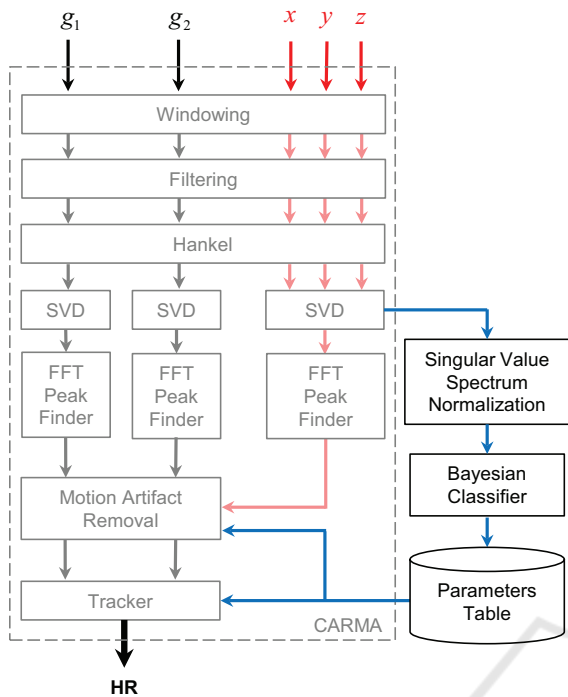


Figure 2: Flow chart of proposed framework (g_1 and g_2 are the PPG channels, x, y, z are the 3-axial accelerometer signals).

4 COMBINING CARMA AND PHYSICAL EXERCISE IDENTIFICATION ALGORITHMS

A schematic diagram of the framework adopted for MA reduction combining both CARMA and physical exercise identification algorithm, is shown in Fig. 2.

By denoting with $H_t \in \mathbb{R}^{N \times 3L}$ the data matrix of the accelerometer signals at each time instant t the HR h_t is estimated, in order to apply the physical exercise identification algorithm, a feature vector ξ_t has to be derived from this matrix.

We noticed that different types of exercises lead to different distributions of the energy of the accelerometer signals among its eigenvectors. Thus, a suitable candidate for identifying the type of exercise is the normalized spectrum of singular values $\Lambda = [\lambda_1 \dots \lambda_N]$, so as to avoid dependence on the intensity of the exercise. Therefore we choose $\xi_t = \Lambda_t / \|\Lambda_t\|$ where $\|\cdot\|$ represents the norm of a vector.

This normalized singular value spectrum can easily be computed immediately after having performed the SVD on the accelerometer signals, and used as input to the Bayesian classifier after a KLT-based dimensionality reduction from $N = 400$ to $M = 10$. The output of the classifier is used to choose the param-

Table 1: Performance (sensitivity, specificity, precision, and accuracy) of the exercise type identifier evaluated on the whole testing set.

class	sens.	spec.	prec.	acc.
1	84.94%	92.02%	93.56%	87.94%
2	92.02%	84.94%	81.74%	87.94%

eters of both the MA remover and the HR tracker, by looking them up on a hand-tuned table carefully written for each exercise type. For instance, exercises involving running require stronger MA removal, thus the dimension of SMS P is set to 10 for them, and just to 2 for other types. Running also require second-harmonic detection, while this is unnecessary for other exercises. A number of other tracking parameters need also be tuned accordingly.

Since the detection of the exercise type is performed for every frame, the tracking parameters are adjusted on the fly and the subject is free to move from one exercise to another, and the system will try to follow.

5 EXPERIMENTAL RESULTS

The experiments were carried out on datasets recorded when subjects performed two different physical exercises. A total of 23 signals were available (Zhang et al., 2015), 12 recorded while subjects performed running drills (classified as type 1 exercise), 11 recorded while subjects performed a mixture of other activities (classified as type 2 exercise). Of these, the first 6 of each class were used for training the classifier, the others for testing purposes. The signals, sampled at 125 Hz were processed using a sliding window 8 s long (corresponding to $W = 1000$ samples), shifted by 2 s for each frame. The Hankel matrices were built using $N = 400$ so that $L = W - N + 1 = 601$.

A first test was devoted to check the effectiveness of the chosen motion eigenvalue spectrum as a significant feature to discriminate the exercise type. Results are shown in Table 1, and we deem an accuracy approaching 88% to be satisfactory, especially since in many signals there are tails where the subject stood essentially still, making classification there quite pointless. For reference, the two classes were modeled using just 5 and 6 Gaussians in the GMM.

The final test involved executing the complete algorithm on all the available data. The average HR error for each signal is reported in Table 2. The upper two blocks report results obtained without using the automatic classifier, and setting the tracking parameters to those optimized for class 1 and class 2

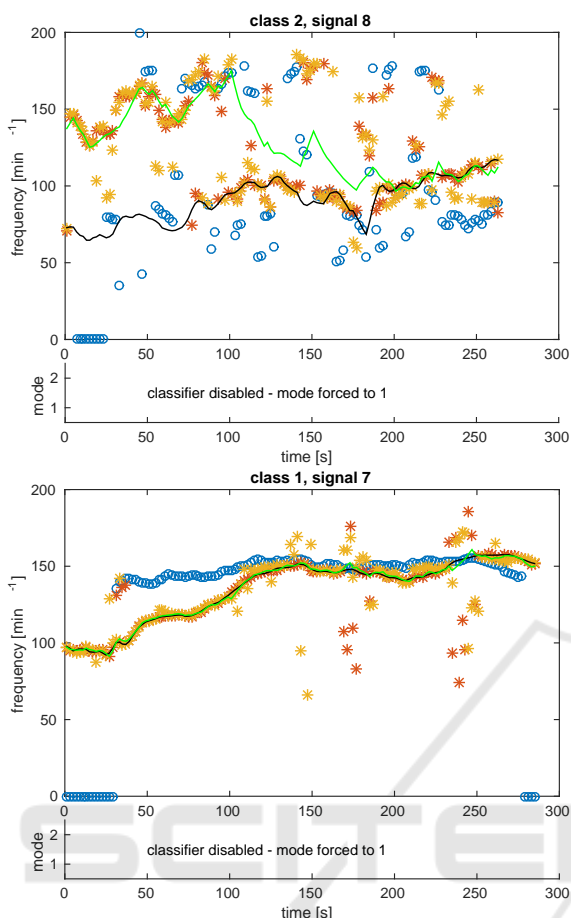


Figure 3: Example of tracking obtained with CARMA alone.

respectively. The bottom block reports the results obtained with the proposed automatic classifier. As can be seen, it nearly always succeeds in selecting the best of the two results.

Moreover, Figs. 3 and 4 show the algorithm tracking capabilities respectively without and with automatic parameter selection for a couple of significant cases.

In these figures, black lines represent the reference (true) HR obtained by simultaneous ECG recordings, the green lines are the estimate obtained by the proposed algorithm. Colored stars represent the frequencies of the spectral peaks extracted from the singular vectors (only first two are shown) which remain after MA removal. These are the values the tracking algorithm tries to follow. Blue circles are the MA frequencies (only the strongest is shown). The bottom pane of each figure shows the automatically identified exercise type for each input frame. As can be seen, most errors occur only during the initial stage of the exercise or when the subject is at rest (low or null MA frequency).

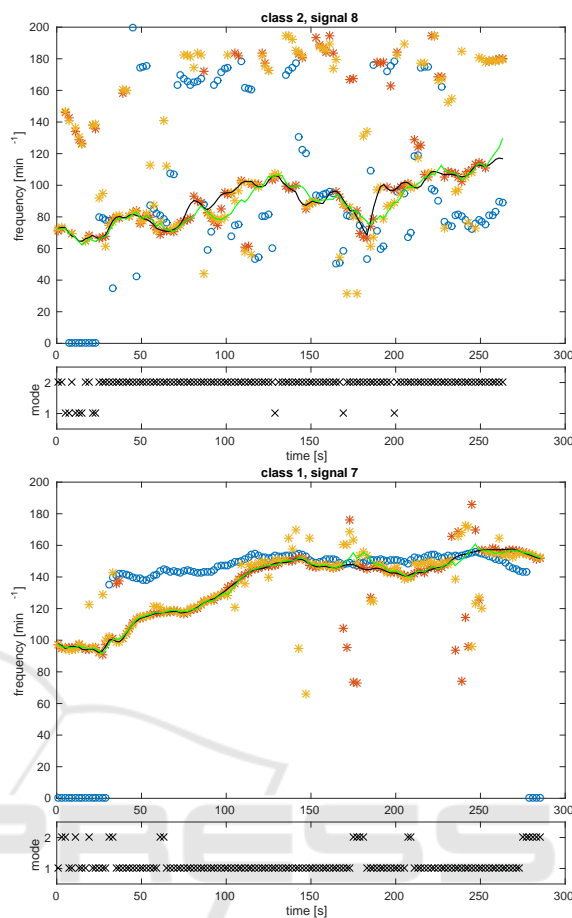


Figure 4: Example of tracking obtained combining CARMA and exercise identification algorithm.

As can be seen e.g. in the top plot of Fig. 3, without the classifier the tracker might be driven off-track when the subject performs a different exercise, leading to huge errors. This does not happen with the classifier enabled, as can be seen in the top plot of Fig. 4. Unfortunately, there can be some points where the classification fails (bottom plot of Fig. 4), but this does not cause the tracker to go completely astray and the loss in accuracy is contained.

A summary of the results, reporting the average tracking error over the whole datasets, are shown in Table 3.

These results clearly show that once the mode is set (corresponding to a tracking model specifically optimized for a single physical exercise) the minimum mean error the CARMA algorithm is able to reach is 10.25 BPM (with mode set to 1), while using the physical exercise identification algorithm the mean error drastically drops to 5.60 BPM.

Of course, the automatic exercise classifier cannot be expected to improve tracking results for the class of signals that matches the one for which the fixed-

Table 2: Average tracking error for the different signals. Shaded cells represents signals that were also used in the training of the classifier.

class	Heart Rate Error [BPM] — without classifier — mode fixed at 1											
	1	2	3	4	5	6	7	8	9	10	11	12
1	2.58	1.48	1.40	2.47	1.54	3.24	1.01	1.19	0.93	6.28	1.68	3.30
2	4.01	30.16	54.94	14.24	25.20	6.63	4.15	38.20	16.10	3.66	1.03	

class	Heart Rate Error [BPM] — without classifier — mode fixed at 2											
	1	2	3	4	5	6	7	8	9	10	11	12
1	15.01	21.91	41.52	3.62	1.53	37.71	3.51	21.01	0.98	67.50	1.70	4.41
2	8.50	20.70	2.85	9.05	23.09	6.62	3.48	3.98	18.12	3.37	1.01	

class	Heart Rate Error [BPM] — with automatic classifier											
	1	2	3	4	5	6	7	8	9	10	11	12
1	3.37	2.79	1.76	2.49	1.54	3.44	1.28	1.84	0.96	6.65	1.64	3.41
2	8.32	13.65	2.86	9.06	23.88	7.15	3.63	3.98	17.58	3.38	1.02	

Table 3: Performance of the HR tracker evaluated on the whole dataset with the original CARMA algorithm and with and without the addition of the exercise type classifier. Data are in beats per minute.

class	mode 1	mode 2	automatic
	error	error	error
1	2.26	18.37	2.60
2	18.03	9.16	8.59
mean	10.15	13.77	5.60

mode algorithm was optimized, though a minor improvement was still achieved for class 2, which comprises a variety of exercises which might sometimes resemble running (class 1). For the first class, only a minor increase in the average error occurs due to a few misclassified frames, but the average error of the two classes still manifest a significative improvement.

6 CONCLUSIONS

In this paper we propose a general framework to reduce MA in PPG when subjects perform various physical exercises.

Experimental results show that currently adopted algorithms for artifact removal behave well when subjects perform a single exercise, while fail when subjects perform various physical exercises.

Using the physical exercise identification algorithm proposed in this work gives a significative improvement (more than 50%) in the average error of the HR estimation for different classes of exercises.

REFERENCES

Bacà, A., Biagetti, G., Camilletti, M., Crippa, P., Falaschetti, L., Orcioni, S., Rossini, L., Tonelli, D.,

and Turchetti, C. (2015). CARMA: A robust motion artifact reduction algorithm for heart rate monitoring from PPG signals. In *23rd European Signal Processing Conference (EUSIPCO 2015)*, pages 2696–2700.

Biagetti, G., Crippa, P., Curzi, A., Orcioni, S., and Turchetti, C. (2015). Speaker identification with short sequences of speech frames. In *4th International Conference on Pattern Recognition Applications and Methods (ICPRAM 2015)*, volume 2, pages 178–185.

Figueiredo, M. A. F. and Jain, A. K. (2002). Unsupervised learning of finite mixture models. *IEEE Transactions on Pattern Analysis and Machine Intelligence*, 24(3):381–396.

Foo, J. Y. A. (2006). Comparison of wavelet transformation and adaptive filtering in restoring artefact-induced time-related measurement. *Biomedical Signal Processing and Control*, 1(1):93–98.

Fukunaga, K. (1990). *Introduction to statistical pattern recognition*. Academic Press.

Gibbs, P. T., Wood, L. B., and Asada, H. H. (2005). Active motion artifact cancellation for wearable health monitoring sensors using collocated MEMS accelerometers. In *Smart Structures and Materials*, volume 5765, pages 811–819. International Society for Optics and Photonics.

Jain, A. K., Duin, R. P. W., and Mao, J. (2000). Statistical pattern recognition: A review. *IEEE Transactions on Pattern Analysis and Machine Intelligence*, 22(1):4–37.

Kim, B. S. and Yoo, S. K. (2006). Motion artifact reduction in photoplethysmography using independent component analysis. *IEEE Transactions on Biomedical Engineering*, 53(3):566–568.

Lee, B., Han, J., Baek, H. J., Shin, J. H., Park, K. S., and Yi, W. J. (2010). Improved elimination of motion artifacts from a photoplethysmographic signal using a Kalman smoother with simultaneous accelerometry. *Physiological Measurement*, 31(12):1585.

Raghuram, M., Madhav, K. V., Krishna, E. H., Komalla, N. R., Sivani, K., and Reddy, K. A. (2012).

- HHT based signal decomposition for reduction of motion artifacts in photoplethysmographic signals. In *IEEE Int. Instrumentation and Measurement Technology Conf. (I2MTC)*, pages 1730–1734.
- Raghuram, M., Madhav, K. V., Krishna, E. H., and Reddy, K. A. (2010). Evaluation of wavelets for reduction of motion artifacts in photoplethysmographic signals. In *10th Int. Conf. Information Sciences Signal Processing and their Applications (ISSPA)*, pages 460–463.
- Raghuram, M., Sivani, K., and Reddy, K. A. (2014). E2MD for reduction of motion artifacts from photoplethysmographic signals. In *Int. Conf. Electronics and Communication Systems (ICECS)*, pages 1–6.
- Ram, M. R., Madhav, K. V., Krishna, E. H., Komalla, N. R., and Reddy, K. A. (2012). A novel approach for motion artifact reduction in PPG signals based on AS-LMS adaptive filter. *IEEE Transactions on Instrumentation and Measurement*, 61(5):1445–1457.
- Reynolds, D. and Rose, R. (1995). Robust text-independent speaker identification using Gaussian mixture speaker models. *IEEE Transactions on Speech and Audio Processing*, 3(1):72–83.
- Zhang, Z., Pi, Z., and Liu, B. (2015). TROIKA: A general framework for heart rate monitoring using wrist-type photoplethysmographic signals during intensive physical exercise. *IEEE Transactions on Biomedical Engineering*, 62(2):522–531.

